Hydrogen-Bond-Dynamics-Based Switching of Conductivity and Magnetism: A Phase Transition Caused by Deuterium and Electron Transfer in a Hydrogen-Bonded Purely Organic Conductor Crystal

Akira Ueda,*,[†] Shota Yamada,[†,‡] Takayuki Isono,[†,¶] Hiromichi Kamo,[†] Akiko Nakao,[§] Reiji Kumai,[∥] Hironori Nakao,[∥] Youichi Murakami,[∥] Kaoru Yamamoto,[⊥] Yutaka Nishio,[‡] and Hatsumi Mori*,[†]

[†]The Institute for Solid State Physics, The University of Tokyo, Kashiwa, Chiba 277-8581, Japan

[‡]Department of Physics, Faculty of Science, Toho University, Funabashi, Chiba 274-8510, Japan

[§]Comprehensive Research Organization for Science and Society (CROSS), Tokai, Ibaraki 319-1106, Japan

[∥]CMRC and Photon Factory, Institute of Materials Structure Science, High Energy Accelerator Research Organization (KEK), Tsukuba, Ibaraki 305-0801, Japan

[⊥]Department of Applied Physics, Okayama University of Science, Okayama 700-0005, Japan

S *Supporting Information*

ABSTRACT: A hydrogen bond (H-bond) is one of the most fundamental and important noncovalent interactions in chemistry, biology, physics, and all other molecular sciences. Especially, the dynamics of a proton or a hydrogen atom in the H-bond has attracted increasing attention, because it plays a crucial role in (bio)chemical reactions and some physical properties, such as dielectricity and proton conductivity. Here we report unprecedented H-bond-dynamics-based switching of electrical conductivity and magnetism in a H-bonded purely organic conductor crystal, κ-D_3(Cat-EDT-TTF)$_2$ (abbreviated as κ-**D**). This novel crystal κ-**D**, a deuterated analogue of κ-H_3(Cat-EDT-TTF)$_2$ (abbreviated as κ-**H**), is composed only of a H-bonded molecular unit, in which two crystallographically equivalent catechol-fused ethylenedithiotetrathiafulvalene (Cat-EDT-TTF) skeletons with a +0.5 charge are linked by a symmetric anionic $[O \cdots D \cdots O]^{-1}$-type strong H-bond. Although the deuterated and parent hydrogen systems, κ-**D** and κ-**H**, are isostructural paramagnetic semiconductors with a dimer-Mott-type electronic structure at room temperature (space group: $C2/c$), only κ-**D** undergoes a phase transition at 185 K, to change to a nonmagnetic insulator with a charge-ordered electronic structure (space group: $P\bar{1}$). The X-ray crystal structure analysis demonstrates that this dramatic switching of the electronic structure and physical properties originates from deuterium transfer or displacement within the H-bond accompanied by electron transfer between the Cat-EDT-TTF π-systems, proving that the H-bonded deuterium dynamics and the conducting TTF π-electron are cooperatively coupled. Furthermore, the reason why this unique phase transition occurs only in κ-**D** is qualitatively discussed in terms of the H/D isotope effect on the H-bond geometry and potential energy curve.
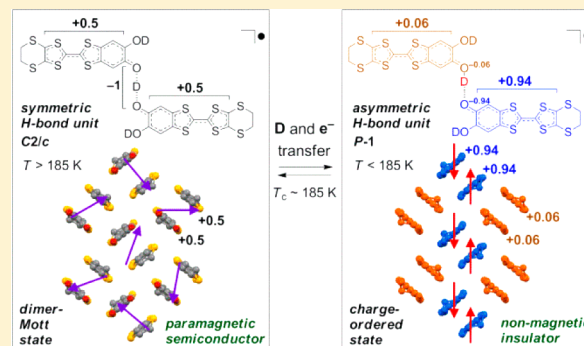
■ INTRODUCTION

A hydrogen bond (H-bond) is one of the most fundamental and important noncovalent interactions in materials and thus has played an essential role in chemistry, biology, physics, and all other molecular sciences, because of its inherent ability to form a wide variety of structures, depending on the constituent elements, geometry, charge, temperature, states of matter, and so on.[1−7] From the geometric viewpoint, the H-bond distance or the interatomic distance between the participating heavy atoms (oxygen, nitrogen, sulfur, halogen, etc.) is a particularly important parameter. This is because, depending on that distance, the shape of the potential curve or the dynamics of the proton (or hydrogen atom) in the H-bond is sensitively changed.[8] For example, in several isostructural series of OHO-type H-bonded dielectrics, their phase transition temperature (T_c), which corresponds to the

thermal order−disorder behavior of the H-bonded proton (or hydrogen atom), increases with increasing $O \cdots O$ distance (d_{OO}).[9−11] In particular, the significant increase of T_c is observed when the H-bonded hydrogen is deuterated, in which the increase in d_{OO} by deuteration, i.e., the so-called geometric isotope effect[12,13] or the Ubbelohde effect,[14] is believed to play an important role.[9−11] Furthermore, the deuteration sometimes induces a new phase transition which is absent in the parent hydrogen system.[15,16] The origin of this so-called deuteration-induced phase transition has been discussed from both the experimental geometric aspect[17] and the theoretical aspect[18−20] which takes into account the difference in zero-point energy.
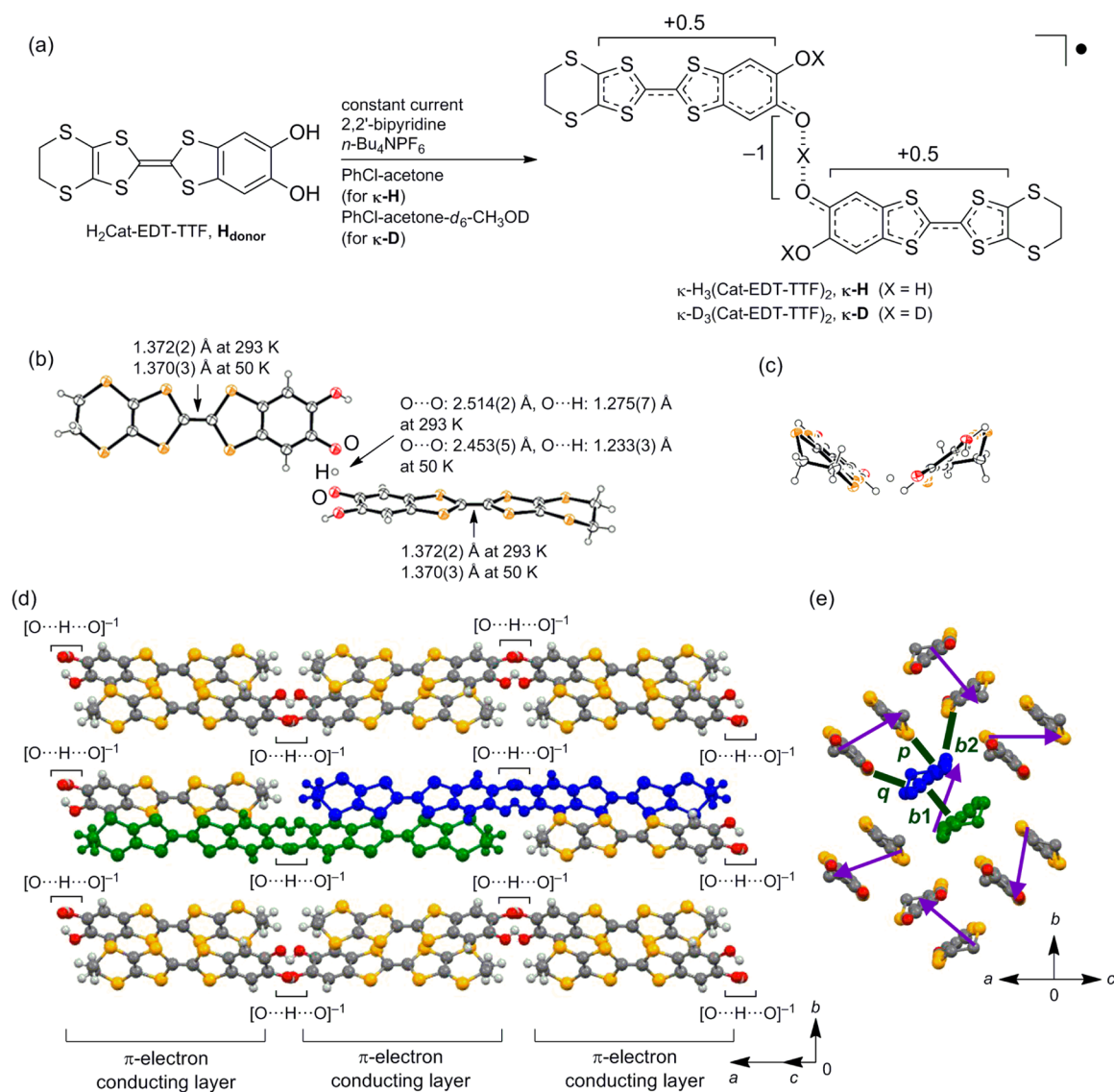
Figure 1. (a) Synthetic scheme of **κ-H**[35] and **κ-D**. (b) Top and (c) side view of the H-bonded molecular unit in the crystal of **κ-H** and its molecular arrangement (d) along the molecular long axis and (e) within the κ-type two-dimensional conducting layer. In (b), values represent the bond lengths or interatomic distances. In (b), (c), the thermal ellipsoids are scaled to the 50% probability level. In (e), $b1$, $b2$, p, and q represent intermolecular transfer integrals within and between the π-dimer(s), respectively ($b1 = 213$ meV, $b2 = 78$ meV, $p = 41$ meV, $q = -16$ meV at 293 K and $b1 = 230$ meV, $b2 = 85$ meV, $p = 46$ meV, $q = -12$ meV at 50 K).

Importantly, all of the above-mentioned interesting dielectric properties are fundamentally attributable to the proton (or hydrogen atom) dynamics in the H-bond, and thus, conversely, the electrons are not relevant to these dynamic properties.

Cooperative behavior between a proton (or a hydrogen atom) and an electron has frequently been observed in a wide variety of biological and chemical processes.[21] For example, in the photosynthetic reaction center, the electron is transported by a sequential proton–electron transfer reaction through a p-benzoquinone derivative, plastoquinone.[22] Importantly, in this reaction, the proton- and electron-accepting abilities of the π-electronic benzoquinone molecule play a vital role. Furthermore, such cooperation between an H-bonded proton (or a hydrogen atom) and an electron is also observed in molecular materials. Quinhydrone, the p-benzoquinone–hydroquinone organic 1:1 cocrystal, exhibits a cooperative proton–electron transfer, based on the coupling of the charge-transfer interaction and H-bond dynamics between the two

organic π-electron components.[23,24] However, high pressure (~25 kbar) is required for the realization of the proton–electron transferred state, and thus a detailed investigation has not been achieved. In addition, several kinds of possible candidates were prepared;[25–34] however, such "dynamic" coupling phenomena between H-bond dynamics and electrons in the solid state have scarcely been observed to date.[26,31]

Recently, our group originally prepared an H-bonded-molecular-unit-based purely organic conductor crystal, κ-H$_3$(Cat-EDT-TTF)$_2$ (abbreviated as **κ-H**)[35] (Figure 1a), in which two crystallographically equivalent catechol-fused ethylenedithiotetrathiafulvalene (Cat-EDT-TTF) skeletons with a +0.5 charge are linked by a symmetric anionic $[O\cdots H\cdots O]^{-1}$-type strong H-bond ($d_{OO} = 2.486(5)$ Å at 293 K, $d_{OO} = 2.453(5)$ Å at 50 K) (Figure 1b,c). Notably, the conductor **κ-H** is composed only of this H-bonded neutral open-shell molecular unit, which enabled the construction of an unprecedented packing structure where the two-dimensional (so-called κ-type) π-electron

conducting layers are connected by the H-bonds (Figure 1d,e). Thus, a significant interplay between the H-bond dynamics and π-electron is expected in this system. Here we report unprecedented H-bond-dynamics-based switching of electrical conductivity and magnetism in a deuterated analogue of this H-bonded purely organic conductor system, κ-D$_3$(Cat-EDT-TTF)$_2$ (abbreviated as **κ-D**, Figure 1a). Although the deuterated and parent hydrogen systems, **κ-D** and **κ-H**, are isostructural paramagnetic semiconductors with a dimer-Mott-type electronic structure at room temperature, only **κ-D** undergoes a phase transition at 185 K, to change to a nonmagnetic insulator with a charge-ordered (CO) electronic structure. The X-ray crystal structure analysis demonstrates that this dramatic switching of the π-electronic structure and physical properties originates from deuterium transfer or displacement within the $[O \cdots D \cdots O]^{-1}$ H-bond accompanied by electron transfer between the H-bonded Cat-EDT-TTF π-systems, proving that the H-bonded deuterium dynamics and the conducting TTF π-electron are cooperatively coupled. Furthermore, the reason why this unique phase transition occurs only in **κ-D** is qualitatively discussed in terms of the H/D isotope effect on the H-bond geometry and potential energy curve.

■ EXPERIMENTAL SECTION

Preparation of D$_3$(Cat-EDT-TTF)$_2$, κ-D. The parent donor H$_2$Cat-EDT-TTF, **H$_{donor}$**[36] (12.0 mg, 0.032 mmol), and 2,2′-bipyridine (15.0 mg, 0.096 mmol) were placed in one side of an H-shaped cell equipped with a glass filter. Then, n-Bu$_4$NPF$_6$ (20 mg) was placed in each side of the cell and the cell was purged by argon gas. These materials were dissolved in a mixed solvent of chlorobenzene (17 mL), acetone-d$_6$ (2 mL, 99.9 atom % D), and CH$_3$OD (0.4 mL, 99.5 atom % D) by sonication. Finally, two annealed Pt electrodes were inserted into the solution and a constant current of 0.3 μA was applied for 1 week at 30 °C, to give black plate crystals of **κ-D** (∼2 mg) which were suitable for the X-ray crystal analysis and physical property measurements. [The deuteration ratio of the **κ-D** crystals is estimated to be over 99% from the X-ray reflection peak intensity ratio between the low-temperature (LT) and high-temperature (HT) phases at 50 K (Figure 3a, see below), on the assumption that the peak intensity for the residual HT-phase is attributable to the contaminant **κ-H** species. Also, the estimation of the deuteration ratio by IR spectroscopy was not successful: The signals attributable to the O–D or O–H vibration were not clearly observed in the IR spectra measured in KBr pellets at room temperature, due to the broad absorption band (probably the charge-transfer band) covering the 1500–3500 cm^{-1} region.]

Preparation of H$_3$(Cat-EDT-TTF)$_2$, κ-H. The crystals of **κ-H** were prepared according to our previous paper.[35]

X-ray Crystal Structure Analysis. X-ray diffraction experiments were performed by using a synchrotron radiation source (λ = 1.0 Å) at the Photon Factory (PF) BL-8A in the High Energy Accelerator Research Organization (KEK), Japan. The diffraction data were collected on an Imaging plate system (Rigaku) equipped with a cold helium gas flow-type system for low-temperature experiments. The crystal structures were solved by direct methods using the SIR2004 program.[37] Refinements were carried out by a full-matrix least-squares method (SHELXL-97),[38] in which all non-hydrogen and hydrogen atoms were refined anisotropically and isotropically, respectively. CCDC-1001782 (**κ-D** at 270 K) and -1001781 (**κ-D** at 50 K) contain the supplementary crystallographic data for this paper. These data can be obtained free of charge from The Cambridge Crystallographic Data Centre via www.ccdc.cam.ac.uk/data_request/cif.

Theoretical Calculations. All DFT calculations mentioned in the text were performed with Gaussian 03, revision E.01.[39] Band structure calculations were performed with the extended Hückel method by using the tight-binding approximation.[40] The molecular geometries of

the H-bonded molecular unit of **κ-D** and **κ-H**[35] were taken from the X-ray analysis data.

Electrical Resistivity. Electrical resistivity measurements of a single crystal of **κ-D** were performed on a Physical Properties Measurement System (PPMS, Quantum Design) by the conventional four-probe method using carbon paste and annealed Au wires (ϕ = 10 μm).

Magnetic Susceptibility. The magnetic susceptibility of a polycrystalline sample of **κ-D** was measured on a Quantum Design SQUID magnetometer MPMS-XL in the temperature range 2−300 K at the static field of 1 T. The magnetic responses were corrected with the blank data of the sample holder obtained separately. The diamagnetic contribution of the sample itself was estimated to be −3.73 × 10^{-4} emu/mol from Pascal's constants.

Raman Spectroscopy. The Raman spectra of a single crystal of **κ-D** and **κ-H** were measured on a Renishaw inVia Reflex Raman microscope (excitation wavelength λ = 633 or 532 nm) at the Institute for Molecular Science, Japan.

■ RESULTS AND DISCUSSION

High-quality single crystals of the deuterated analogue **κ-D** were readily prepared from H$_2$Cat-EDT-TTF, **H$_{donor}$**,[36] in a one-step one-pot synthesis (Figure 1a): Applying a constant current (0.3 μA, about 1 week) to **H$_{donor}$** in a mixed solvent of PhCl–acetone-d$_6$–CH$_3$OD including 2,2′-bipyridine and n-Bu$_4$NPF$_6$ gave **κ-D** as black crystals, through H/D exchange of the catechol hydroxyl groups, oxidation of the TTF skeletons, and H-bond unit formation. The crystals **κ-D** are quantitatively deuterated (according to Figure 3a, see below) and can be stably stored for a long time under moisture-free conditions. However, under air the deuteration ratio gradually lowers in a few weeks, probably due to the D/H exchange by atmospheric H$_2$O.

In order to examine how the H/D substitution affects the physical properties of this system, we have first measured the electrical resistivity (ρ) of **κ-D** as a function of temperature. As displayed in Figure 2a, ρ of a single crystal of **κ-D** (blue circles) monotonically increased with decreasing temperature from 300 to 182 K, showing typical semiconducting behavior similar to that of the parent **κ-H** (black circles).[35] The room-temperature electrical conductivity σ_{rt} (= $1/\rho_{rt}$) and activation energy E_a of **κ-D** (6.2 S cm^{-1}, 0.08 eV) are, however, slightly higher and lower than those of **κ-H** (3.5 S cm^{-1}, 0.11 eV), respectively, probably due to the so-called chemical pressure effect by deuteration[41] (for the crystallographic parameters, see Table S1 in the Supporting Information). Upon further cooling, **κ-D** showed a rapid increase in ρ at 182 K, to undergo a semiconductor−insulator-like phase transition, which is in sharp contrast to the continuous monotonic semiconducting behavior in **κ-H**. Furthermore, a small thermal hysteresis of 4 K (see the inset of Figure 2a) is observed upon heating (red circles) and this temperature dependence is reversible.

Such a remarkable H/D substitution effect is also observed in the temperature dependence of the magnetic susceptibility (χ_p) of **κ-D** and **κ-H** in the polycrystalline state in the temperature range 2−300 K (Figure 2b). With decreasing temperature, the χ_p of **κ-H** (black circles) monotonically increases down to around 20 K and then begins to decrease.[42] On the other hand, the deuterated analogue **κ-D** (blue circles) exhibits an abrupt drop of χ_p at 185 K after the monotonic increase similar to that for **κ-H**. Importantly, the temperature at which the anomaly of χ_p occurs is similar to that of ρ (Figure 2a), indicating that the origin of these anomalies is the same. After the abrupt drop, the χ_p of **κ-D** gradually approaches ∼0.0 emu mol^{-1} with decreasing temperature. This low-temperature magnetic behavior is reproduced by the singlet−triplet dimer model[43]
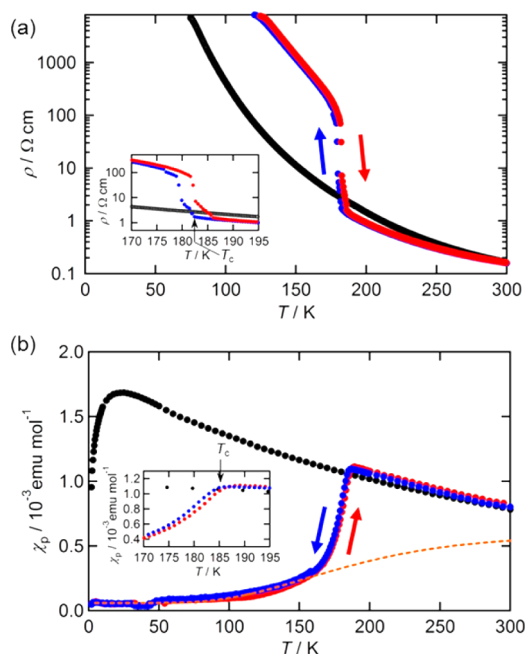
Figure 2. Temperature dependence of (a) electrical resistivity (on a single crystal) and (b) magnetic susceptibility (of a polycrystalline sample) of κ-**D** (blue and red circles represent the cooling and heating processes, respectively) and κ-**H**[35,42] (black circles in the cooling process). In (b), the Curie contribution (0.5% for κ-**D** and 0.6% for κ-**H**) is subtracted from the original data, and the anomaly at around 40 K in κ-**D** is attributed to the presence of molecular oxygen in the sample holder. The orange line represents the fitting curve for κ-**D** by the singlet−triplet dimer model[43] with an antiferromagnetic coupling of $2J/k_B \approx -600$ K.

with an antiferromagnetic coupling of $2J/k_B \approx -600$ K (orange line in Figure 2b). Therefore, a spin-singlet state is formed in κ-**D** by the magnetic transition from the high-temperature (HT) paramagnetic phase, which leads to a nonmagnetic ground state, in sharp contrast to κ-**H** with a quantum spin liquid ground state.[42] Furthermore, this transition is accompanied by a small hysteresis (~1 K), as seen in the resistivity measurement (Figure 2a), thus suggesting that this is a first-order phase transition. Importantly, the fact that the modulation of the H-bond nature by H/D substitution causes the phase transition accompanied by significant switching of electrical conductivity and magnetism suggests that the H-bond dynamics and the TTF π-electronic system are strongly coupled in the crystalline state. Furthermore, since this phase transition does not occur in κ-**H** down to 50 mK,[42] one can see that the transition temperature T_c of κ-**D** increases by about 185 K by the $[O{\cdots}D{\cdots}O]^{-1}$ deuteration. Although a similar kind of deuteration-induced T_c increase by 50−150 K is sometimes observed in H-bonded inorganic[9−12,15−17] and organic[28,44,45] crystals, such a surprisingly large increase in T_c by over 180 K has not been reported, to our knowledge.

In order to gain structural insight into this deuteration-induced phase transition with the conductivity and magnetism switching, we have carried out X-ray diffraction studies on a single crystal of κ-**D** using synchrotron radiation in the temperature range of 50−270 K. At 270 K, κ-**D** is found to be isostructural with κ-**H** at 293 K[35] (see Table S1 in Supporting Information): The κ-**D** system at 270 K crystallizes in the $C2/c$ space group and is composed of an $[O{\cdots}D{\cdots}O]^{-1}$ H-bonded molecular unit having two crystallographically equivalent

Cat-EDT-TTF$^{+0.5}$ skeletons (Figure 3b left). We should note that the H-bonded O$\cdots$O distance in κ-**D** (2.501(2) Å at 270 K, Figure 3c left) is significantly elongated compared to that in κ-**H** (2.486(5) Å at 293 K, Figure 1b),[35] due to the so-called geometric isotope effect[12,13] or Ubbelohde effect;[14] however, there are no marked differences in the bond lengths, molecular arrangement, and intermolecular transfer integrals of the Cat-EDT-TTF skeletons of these systems (Figure 1b−e, 3b left, and 4b left). As a result, in the HT phase ($T = 185−300$ K), κ-**D** exhibits similar physical properties to those of κ-**H**, as shown in Figure 2a,b. On the other hand, the low-temperature (LT) crystal structures of κ-**D** and κ-**H** are completely different from each other. The hydrogen compound κ-**H** maintains its room-temperature crystal structure with $C2/c$ symmetry even at 50 K, whereas the deuterated κ-**D** abruptly starts to produce a new phase with $P\bar{1}$ symmetry at around 180 K and then the original HT phase almost completely disappears (<1%) at 160 K (Figure 3a). Importantly, the temperature when the LT phase appears (~180 K) agrees well with the T_c observed in the electrical resistivity (182 K, Figure 2a) and magnetic susceptibility (185 K, Figure 2b), thus strongly suggesting that the phase transition occurs in association with this crystal structure change. Also, the complete and rapid disappearance of the HT phase indicates that the prepared κ-**D** single crystals are almost completely deuterated, because reflections attributable to the HT phase would more slowly disappear or remain even at low temperatures if some κ-**H** species are involved in the crystal as a contaminant.

Thus, we next determined the crystal structure of the LT phase of κ-**D** by using the diffraction data at 50 K (Figures 3b−e right and 4a, 4b right). Upon the phase transition, the H-bonded deuterium transfers from the center of the two oxygen atoms toward one oxygen atom, to form an asymmetric $[O{-}D{\cdots}O]^{-1}$ H-bond with short O−D (1.02(5) Å) and long O$\cdots$D (1.51(5) Å) distances (Figure 3c right), instead of the two equivalent O$\cdots$D distances at 270 K (1.265(7) Å, Figure 3c left). This asymmetrization is clearly observed in the difference Fourier maps (Figure S2 in Supporting Information). As a result, the two crystallographically equivalent Cat-EDT-TTF$^{+0.5}$ skeletons in the HT phase are also desymmetrized, to give a charge-poor Cat-EDT-TTF$^{+0.06}$ with the short O−D distance and a charge-rich Cat-EDT-TTF$^{+0.94}$ with the long O$\cdots$D distance (Figure 3b,c), as estimated from the bond lengths of the TTF skeletons (1.344(3) Å vs 1.399(3) Å for the central C=C bond in Figure 3c; see also Table S2 in the Supporting Information for details). These results demonstrate that the H-bonded deuterium transfer or displacement gives rise to the significant charge disproportionation between the H-bonded Cat-EDT-TTF skeletons, proving the presence of an effective coupling between the H-bonded deuterium dynamics and the electron-donating-/accepting ability of the TTF π-system. The plausible mechanism of this charge disproportionation (for details, see Figure S3 in the Supporting Information) is that (1) the H-bonded deuterium transfer gives the asymmetric $[O{-}D{\cdots}O]^{-1}$ H-bond, (2) which induces disproportionation of the negative charge within the H-bond like $O^{-0.06}{-}D{\cdots}O^{-0.94}$, and then (3) intraunit donor−acceptor-type electron transfer occurs from the TTF$^{+0.5}$ skeleton with a more negative H-bond part (the $O^{-0.94}$ atom) to that with a less negative one (the $O^{-0.06}{-}D$ moiety) to compensate the charge neutrality on each molecule, leading to the charge-poor Cat-EDT-TTF$^{+0.06}$ with the $O^{-0.06}{-}D$ moiety and the charge-rich Cat-EDT-TTF$^{+0.94}$ with the $O^{-0.94}$ atom. In fact, the highly charge-disproportionated $O^{-0.06}{-}D{\cdots}O^{-0.94}$ nature is confirmed
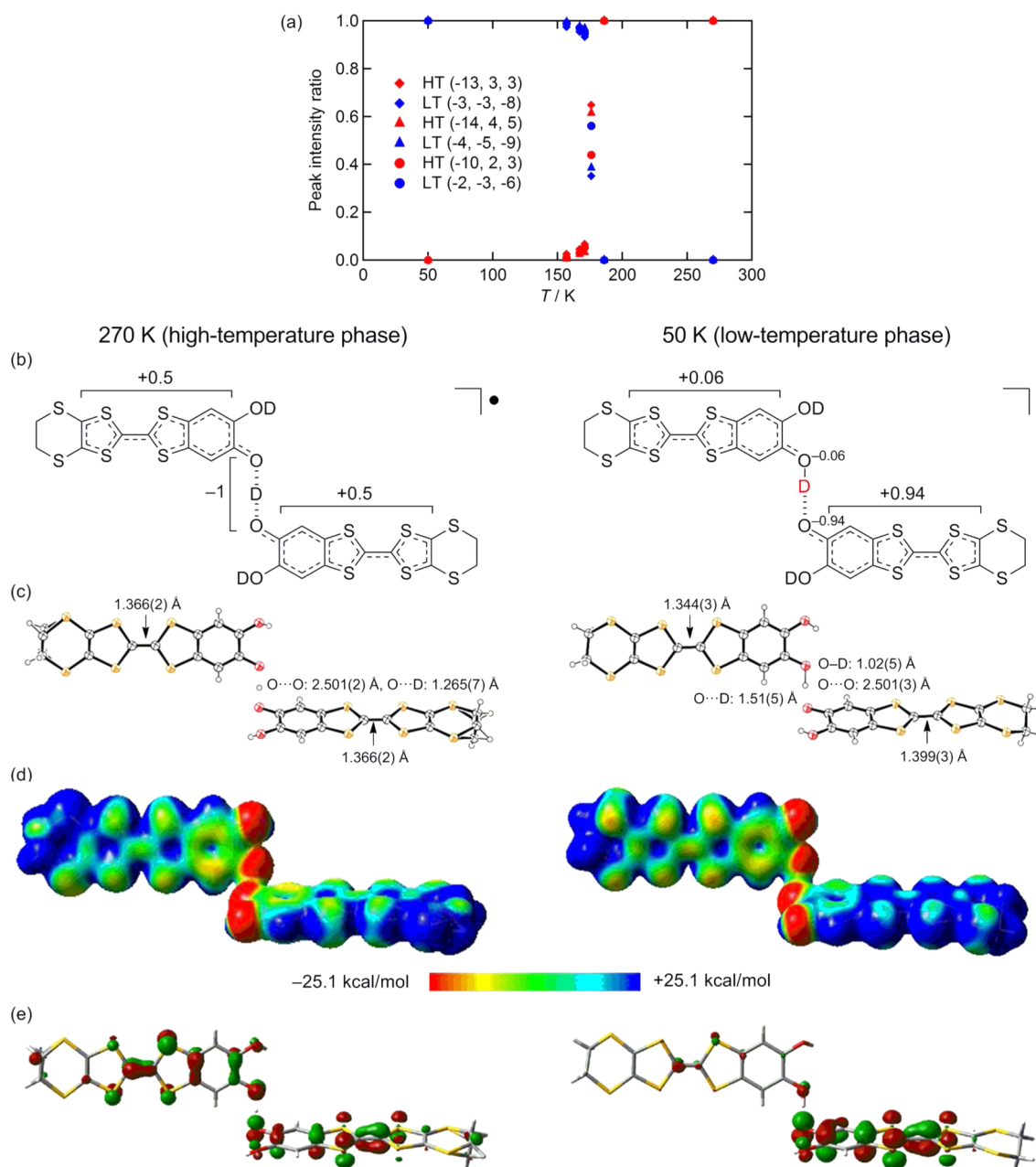
Figure 3. (a) Temperature dependence of relative X-ray reflection intensity for three pairs of peaks from the high-temperature (HT) $C2/c$ phase (red colored) and low-temperature (LT) $P\bar{1}$ phase (blue colored) in a single crystal of κ-D; (squares, (−13, 3, 3), (−3, −3, −8)), (triangles, (−14, 4, 5), (−4, −5, −9)), (circles, (−10, 2, 3), (−2, −3, −6)). (b) Chemical structures, (c) X-ray crystal structures, (d) electrostatic potential surfaces, and (e) SOMO distributions of the H-bonded molecular unit in κ-D at 270 K (left column) and 50 K (right column). At 270 K, the terminal ethylene groups are thermally disordered. Values in (c) are the bond lengths or interatomic distances. In (c), the thermal ellipsoids are scaled to the 50% probability level. Theoretical calculations for (d) and (e) were performed at the UB3LYP/6-31G(d) level of theory and the ROB3LYP/6-31G(d) level of theory, respectively. The molecular geometries used for the calculations were taken from the X-ray analysis data.

by the bond length analysis of the catechol moiety (Figure S4 in Supporting Information). Furthermore, density functional theory (DFT) calculations based on the X-ray structures (Figure 3d,e) also support the occurrence of the charge disproportionation between the H-bonded TTF skeletons. The electrostatic potential surface at 50 K (Figure 3d right) illustrates the presence of a more positively charged TTF skeleton (aqua-to-blue-colored) and a less positively charged one (green-to-yellow-colored), which correspond to the experimental charge-rich (+0.94) and charge-poor (+0.06) skeletons, respectively. Concurrently, almost all of the coefficients of the singly occupied

molecular orbital (SOMO) are found on the Cat-EDT-TTF$^{+0.94}$ skeleton (Figure 3e right). In addition, we successfully observe the charge disproportionation behavior between the TTF skeletons by single-crystal Raman measurements of κ-D and κ-H (Figures S5, S6 in the Supporting Information). The temperature dependence suggests that the charge disproportionated state in κ-D (+0.94 vs +0.06) is directly formed from the initial +0.5 oxidized state without passing through other intermediate states (e.g., +0.7 vs +0.3, etc.).

Due to the above-mentioned intraunit charge disproportionation through the H-bond, the overall electronic structure of
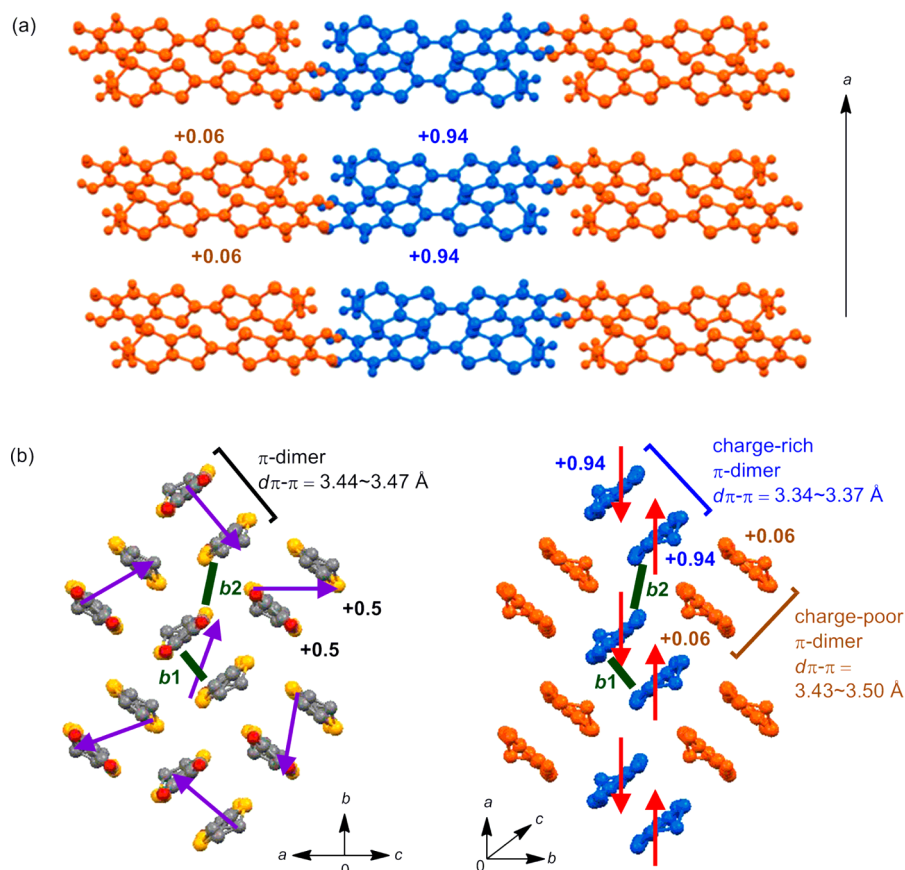
Figure 4. Crystal packing structures of **κ-D**. (a) Molecular arrangement of the Cat-EDT-TTF skeletons between the conducting layers at 50 K and (b) within the conducting layer (left: 270 K, right: 50 K). Blue- and orange-colored molecules correspond to the charge-rich (+0.94) and charge-poor (+0.06) Cat-TTF-skeletons, respectively. The parameters $b1$ and $b2$ in (b) represent intermolecular transfer integrals within and between the π-dimer(s), respectively ($b1 = 218$ meV, $b2 = 79$ meV at 270 K (left) and $b1 = 335$ meV, $b2 = 79$ meV at 50 K (right)).

κ-D in the LT phase is intrinsically different from that in the HT phase. At 50 K, as shown in Figure 4a,b, the charge-rich (blue-colored) and -poor (orange-colored) Cat-EDT-TTF skeletons are separately π-dimerized with their neighboring cofacial Cat-EDT-TTF skeletons having the same valence, to form two kinds of π-dimeric pairs, composed of the charge-rich skeletons or the charge-poor ones. These π-dimers are stacked two-dimensionally while maintaining the κ-type molecular arrangement, which results in a charge-ordered (CO) electronic structure (Figure 4b right) from a dimer-Mott state in the HT phase (Figure 4b left). In this CO state, since the charge-rich TTF$^{+0.94}$ skeleton is expected to have nearly one electron spin ($S = 1/2$), as shown in the SOMO distribution map (Figure 3e right), a spin singlet should be formed within each charge-rich π-dimer, which rationalizes the paramagnetic−nonmagnetic transition in magnetic susceptibility (Figure 2b) as well as the semiconductor−insulator-like transition in resistivity (Figure 2a). Due to the spin-singlet formation, the interplanar distance within the charge-rich π-dimer at 50 K ($d_{\pi-\pi} = 3.34-3.37$ Å) is significantly shortened from that within the original π-dimer at 270 K ($d_{\pi-\pi} = 3.44-3.47$ Å) (Figure 4b), and accordingly the transfer integral within the charge-rich π-dimer ($b1$) at 50 K (331 meV) is greatly enhanced from that within the original one at 270 K (218 meV). Importantly, this CO state is obviously triggered by the H-bonded deuterium transfer, followed by the charge disproportionation, thus which intrinsically differs in its origin from the typical CO state in (BEDT-TTF)$_2$X salts [BEDT-TTF = bis(ethylenedithio)tetrathiafulvalene,

X = monovalent anion],[46−48] derived from the Coulomb interactions between the BEDT-TTF molecules, i.e., the charge degree of freedom of π-electrons. Therefore, the present system is a truly new type of organic CO crystal in which the proton degree of freedom plays a vital role.

Finally, let us discuss why this phase transition occurs not in the parent system **κ-H** but in the deuterated system **κ-D**. We therefore focused on the structural difference in the geometry of the [O···H(D)···O]$^{-1}$ H-bond part of both the systems and calculated the potential energy curves as a function of the distance between the O1···O2 center position and the H-bonded hydrogen or deuterium atom, which moves linearly between O1···O2 (Figure 5). We note here that the calculations were performed on the basis of the X-ray structural data of **κ-H** (293 and 50 K) and **κ-D** (270 and 50 K), in which the deuterium atoms in **κ-D** were replaced with hydrogen atoms to simply estimate the effect due to the geometric difference: The H/D quantum isotope effect relevant to the difference in vibrational frequency was not taken into consideration in the present calculations. At high temperatures, both **κ-H** (Figure 5a, at 293 K) and **κ-D** (Figure 5c, at 270 K) provide a symmetric double-well potential curve, in which the energy barrier for hydrogen transfer is calculated to be 0.09 eV for **κ-H** and 0.14 eV for **κ-D**, respectively. On cooling down to 50 K, **κ-H** still maintains the symmetric potential curve, in which the barrier is lowered to 0.07 eV (Figure 5b). On the other hand, the potential curve of **κ-D** desymmetrizes at 50 K with a much higher barrier (0.26 eV) (Figure 5d), as expected from the
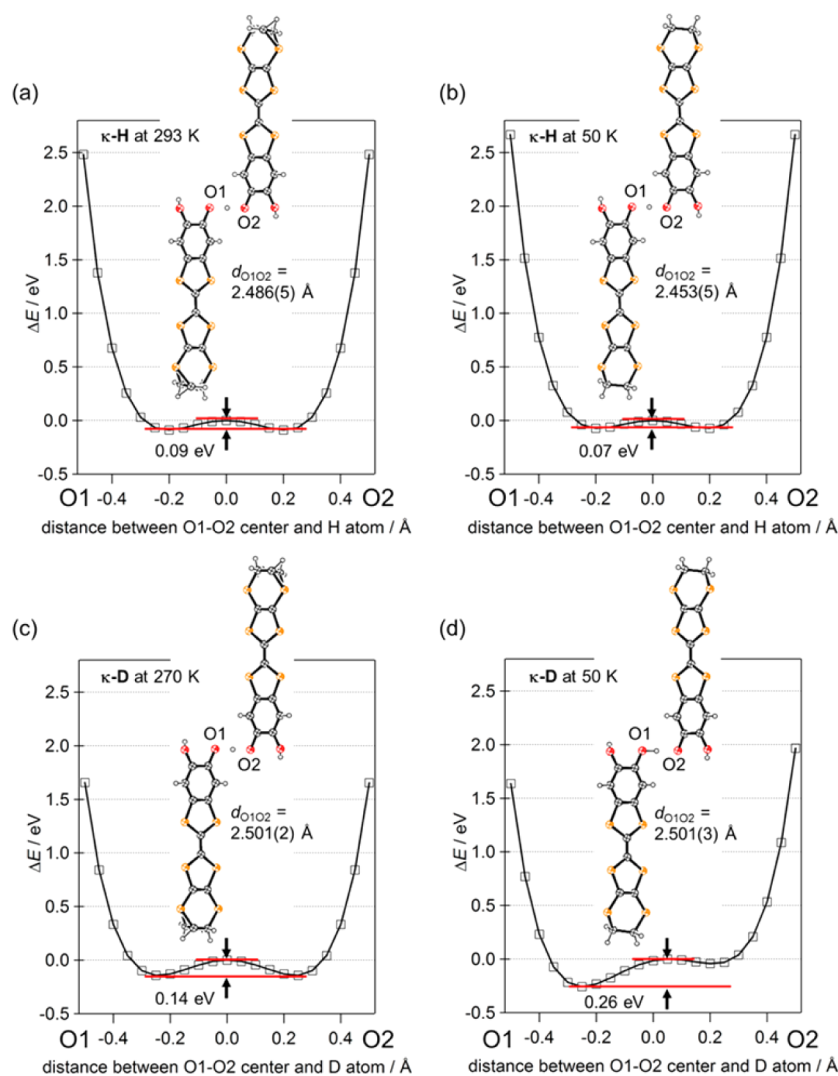
Figure 5. Theoretical potential energy curves for the intraunit H-bond part in **κ-H** and **κ-D**. The total energy profiles (ΔE, in eV) of **κ-H** at (a) 293 K and (b) 50 K and of **κ-D** at (c) 270 K and (d) 50 K as a function of the distance between the O1···O2 center position and the H-bonded proton, which moves linearly between O1···O2. The calculations were performed at the UB3LYP/6-31G(d) level of theory by using the X-ray structural data with changing the H-bonded hydrogen atom position. In these calculations, the deuterium atoms in **κ-D** were replaced with hydrogen atoms: The H/D quantum isotope effect relevant to the difference in zero-point energy was not taken into consideration. In the inset, each H-bonded molecular unit structure in the crystal is shown. The thermal ellipsoids are scaled to the 50% probability level.

asymmetric $O^{-0.06}-D\cdots O^{-0.94}$ H-bond structure. On the basis of these calculated results relevant to the geometric difference, the presence or absence of the phase transition in the **κ-H** and **κ-D** systems can be qualitatively interpreted as follows: (1) At high temperatures, due to the short O1···O2 distance (d_{O1O2}) (2.486(5) Å for **κ-H** and 2.501(2) Å for **κ-D**), the energy barrier in each system is low enough to allow the rapid hydrogen or deuterium transfer between the two potential minima by thermal activation, resulting in the formation of the H- or D-centered $[O\cdots H(D)\cdots O]^{-1}$ structure as a time-averaged X-ray structure. (2) At 50 K, the d_{O1O2} in **κ-H** decreases to 2.453(5) Å by shrinking of the unit cell and thus the energy barrier is further lowered, which enables the hydrogen to continue to transfer between the two minima by zero-point vibration or tunneling, to keep the symmetric $[O\cdots H\cdots O]^{-1}$ structure even at low temperatures. (3) On the other hand, the d_{O1O2} in **κ-D** at 50 K (2.501(3) Å) is almost unchanged from that at 270 K (2.501(2) Å) and is significantly longer than that of **κ-H** at 50 K (2.453(5) Å), which is indicative that the energy barrier in **κ-D** at 50 K is

much higher than that in **κ-H** at 50 K. (4) In addition, due to its lower zero-point energy resulting from the heavier atomic mass, the deuterium at low temperatures would be no longer capable of jumping over the energy barrier, to localize at one minimum site such as $O^{-0.06}-D\cdots O^{-0.94}$, which thus triggers the electron transfer and charge disproportionation between the intraunit TTF skeletons. This discussion suggests that, in the present system, the d_{O1O2} difference due to the H/D substitution, that is, the geometric isotope effect, is one of the key factors determining whether the phase transition occurs or not. According to the literature,[12,13] the elongation of d_{OO} due to this effect is the most remarkable when the d_{OO} is around 2.5 Å. Actually, the d_{OO} of the present systems **κ-H** and **κ-D** (2.45–2.50 Å) are in a similar range, which leads to the large elongation in d_{OO} (0.015 Å at 270–293 K and 0.048 Å at 50 K) upon deuteration. For further detailed understanding of this isotope effect, a sophisticated quantum chemical calculation on the potential energy curve, in which the difference in the quantum nature of these isotopes is taken into consideration,[18–20,49,50] is needed and is currently underway.

CONCLUSIONS

In summary, we have discovered unprecedented H-bond-dynamics-based switching of conductivity and magnetism in a purely organic conductor crystal: Deuteration of the $[O\cdots H\cdots O]^{-1}$ H-bond in a catechol-fused TTF-based purely organic conductor crystal, κ-H_3(Cat-EDT-TTF)$_2$ or κ-H, gives rise to a phase transition at 185 K with significant switching of the π-electronic structure (dimer-Mott $\leftrightarrow$ charge order), electrical conductivity (semiconducting $\leftrightarrow$ insulating), and magnetism (paramagnetic $\leftrightarrow$ nonmagnetic), due to deuterium transfer or displacement within the H-bond accompanied by electron transfer between the H-bonded Cat-EDT-TTF π-systems. This result clearly demonstrates that the H-bonded deuterium dynamics and the TTF π-electron are cooperatively coupled in the present system. In this paper, we propose from the structural viewpoint that the geometric isotope effect in the short symmetric $[O\cdots H(D)\cdots O]^{-1}$ H-bond plays an important role in the occurrence of this phase transition. Meanwhile, the quantum isotope effect relevant to the zero-point energy difference will be fundamentally involved in this phenomenon. Thus, a sophisticated theoretical investigation that takes into account the quantum isotope effect is currently underway for a detailed understanding of its origin and mechanism. Here we emphasize that the successful synthesis of a new type of H-bonded organic conductor, "the H-bonded-molecular-unit-based purely organic conductors" κ-D and κ-H,[35,42] allowed us to perform, for the first time, a molecular-level study on "dynamic" coupling phenomena between the H-bond dynamics and the π-electrons in a crystalline organic conductor. Therefore, further chemical modification of this system is currently underway in our group in order not only to gain further insight into this type of unprecedented solid-state dynamic phenomenon but also to explore novel switchable or stimuli-responsive (multi)functional molecular materials/devices[51] by utilizing H-bond dynamics coupled to π-electronic physical properties.

ASSOCIATED CONTENT

⑤ Supporting Information

Crystallographic data, supporting X-ray structural study, and Raman spectroscopy. This material is available free of charge via the Internet at http://pubs.acs.org.

AUTHOR INFORMATION

Corresponding Authors
a-ueda@issp.u-tokyo.ac.jp
hmori@issp.u-tokyo.ac.jp

Present Address
¶National Institute for Materials Science, Tsukuba, Ibaraki 305-0003, Japan.

Notes
The authors declare no competing financial interest.

ACKNOWLEDGMENTS

REFERENCES

(1) Pauling, L. *The Nature of the Chemical Bond*, 3rd ed.; Cornell University Press: New York, 1960.
(2) Hamilton, W. C.; Ibers, J. A. *Hydrogen Bonding In Solids*; Benjamin: New York, 1968.
(3) Schuster, P.; Zundel, G.; Sandorfy, C. *The Hydrogen Bond, Vols. I–III*; North-Holland Publishing Company: Amsterdam, 1976.
(4) Jeffrey, G. A. *An Introduction to Hydrogen Bonding*; Oxford University Press: New York, 1997.
(5) Desiraju, G. R.; Steiner, T. *The Weak Hydrogen Bond*; Oxford University Press: New York, 1999.
(6) Gilli, G.; Gilli, P. *The Nature of the Hydrogen Bond*; Oxford University Press: New York, 2009.
(7) Streiner, T. *Angew. Chem., Int. Ed.* **2002**, *41*, 48−76.
(8) Hynes, J. T.; Klinman, J. P.; Limbach, H.-H.; Schowen, R. L. *Hydrogen-Transfer Reactions*; Wiley-VCH: Weinheim, 2007.
(9) Ichikawa, M.; Motida, K.; Yamada, N. *Phys. Rev. B* **1987**, *36*, 874−876.
(10) McMahon, M. I.; Nelmes, R. J.; Kuhs, W. F.; Dorwarth, R.; Piltz, R. O.; Tun, Z. *Nature* **1990**, *348*, 317−319.
(11) Ichikawa, M.; Gustafsson, T.; Olovsson, I. *Solid State Commun.* **1993**, *87*, 349−353.
(12) Ichikawa, M. *Acta Crystallogr., Sect. B* **1978**, *34*, 2074−2080.
(13) Ichikawa, M. *J. Mol. Struct.* **2000**, *552*, 63−70.
(14) Ubbelohde, A. R.; Woodward, I. *Proc. R. Soc. A* **1946**, *185*, 448−465.
(15) Gesi, K. *J. Phys. Soc. Jpn.* **1980**, *48*, 886−889.
(16) Morimoto, Y.; Tokura, Y.; Nagaoka, N.; Suzuki, T.; Kumagai, K. *Phys. Rev. Lett.* **1993**, *71*, 2833−2836.
(17) Ichikawa, M.; Matsuo, T. *J. Mol. Struct.* **1996**, *378*, 17−27.
(18) Totsuji, C.; Matsubara, T. *Solid State Commun.* **1994**, *89*, 677−681.
(19) Totsuji, C.; Matsubara, T. *Solid State Commun.* **1998**, *105*, 731−733.
(20) Tachikawa, M. *Integr. Ferroelectr.* **2008**, *100*, 72−78.
(21) Huynh, M. H. V.; Meyer, T. J. *Chem. Rev.* **2007**, *107*, 5004−5064.
(22) Feher, G.; Allen, J. P.; Okamura, M. Y.; Rees, D. C. *Nature* **1989**, *339*, 111−116.
(23) Mitani, T.; Saito, G.; Urayama, H. *Phys. Rev. Lett.* **1988**, *60*, 2299−2302.
(24) Nakasuji, K.; Sugiura, K.; Kitagawa, T.; Toyoda, J.; Okamoto, H.; Okaniwa, K.; Mitani, T.; Yamamoto, H.; Murata, I.; Kawamoto, A.; Tanaka, J. *J. Am. Chem. Soc.* **1991**, *113*, 1862−1864.
(25) Batail, P.; LaPlaca, S. J.; Mayerle, J. J.; Torrance, J. B. *J. Am. Chem. Soc.* **1981**, *103*, 951−953.
(26) Felderhoff, M.; Steller, I.; Reyes-Arellano, A.; Boese, R.; Sustmann, R. *Adv. Mater.* **1996**, *8*, 402−405.
(27) (a) Murata, T.; Morita, Y.; Fukui, K.; Sato, K.; Shiomi, D.; Takui, T.; Maesato, M.; Yamochi, H.; Saito, G.; Nakasuji, K. *Angew. Chem., Int. Ed.* **2004**, *43*, 6343−6346. (b) Morita, Y.; Murata, T.; Nakasuji, K. *Bull. Chem. Soc. Jpn.* **2013**, *86*, 183−197.
(28) Akutagawa, T.; Takeda, S.; Hasegawa, T.; Nakamura, T. *J. Am. Chem. Soc.* **2004**, *126*, 291−294.
(29) Kubo, T.; Ohashi, M.; Miyazaki, K.; Ichimura, A.; Nakasuji, K. *Inorg. Chem.* **2004**, *43*, 7301−7307.
(30) Tadokoro, M.; Inoue, T.; Tamaki, S.; Fujii, K.; Isogai, K.; Nakazawa, H.; Takeda, S.; Isobe, K.; Koga, N.; Ichimura, A.; Nakasuji, K. *Angew. Chem., Int. Ed.* **2007**, *46*, 5938−5942.

12191

dx.doi.org/10.1021/ja507132m | *J. Am. Chem. Soc.* 2014, 136, 12184−12192

(31) Fujioka, J.; Horiuchi, S.; Kagawa, F.; Tokura, Y. *Phys. Rev. Lett.* **2009**, *102*, 197601.

(32) (a) Kobayashi, Y.; Yoshioka, M.; Saigo, K.; Hashizume, D.; Ogura, T. *J. Am. Chem. Soc.* **2009**, *131*, 9995−10002. (b) Terauchi, T.; Sumi, S.; Kobayashi, Y.; Nakamura, T.; Furukawa, K.; Misaki, Y. *Chem. Commun.* **2014**, *50*, 7111−7113.

(33) (a) Lee, S. C.; Ueda, A.; Kamo, H.; Takahashi, K.; Uruichi, M.; Yamamoto, K.; Yakushi, K.; Nakao, A.; Kumai, R.; Kobayashi, K.; Nakao, H.; Murakami, Y.; Mori, H. *Chem. Commun.* **2012**, *48*, 8673−8675. (b) Lee, S. C.; Ueda, A.; Nakao, A.; Kumai, R.; Nakao, H.; Murakami, Y.; Mori, H. *Chem.—Eur. J.* **2014**, *20*, 1909−1917.

(34) El-Ghayoury, A.; Mézière, C.; Simonov, S.; Zorina, L.; Cobián, M.; Canadell, E.; Rovira, C.; Náfrádi, B.; Sipos, B.; Forró, L.; Batail, P. *Chem.—Eur. J.* **2010**, *16*, 14051−14059.

(35) Isono, T.; Kamo, H.; Ueda, A.; Takahashi, K.; Nakao, A.; Kumai, R.; Nakao, H.; Kobayashi, K.; Murakami, Y.; Mori, H. *Nat. Commun.* **2013**, *4*, 1344.

(36) Kamo, H.; Ueda, A.; Isono, T.; Takahashi, K.; Mori, H. *Tetrahedron Lett.* **2012**, *53*, 4385−4388.

(37) Burla, M. C.; Caliandro, R.; Camalli, M.; Carrozzini, B.; Cascarano, G. L.; De Caro, L.; Giacovazzo, C.; Polidori, G.; Spagna, R. *J. Appl. Crystallogr.* **2005**, *38*, 381−388.

(38) Sheldrick, G. M. *Acta Crystallogr., Sect. A* **2008**, *64*, 112−122.

(39) Frisch, M. J.; Trucks, G. W.; Schlegel, H. B.; Scuseria, G. E.; Robb, M. A.; Cheeseman, J. R.; Montgomery, J. A., Jr.; Vreven, T.; Kudin, K. N.; Burant, J. C.; Millam, J. M.; Iyengar, S. S.; Tomasi, J.; Barone, V.; Mennucci, B.; Cossi, M.; Scalmani, G.; Rega, N.; Petersson, G. A.; Nakatsuji, H.; Hada, M.; Ehara, M.; Toyota, K.; Fukuda, R.; Hasegawa, J.; Ishida, M.; Nakajima, T.; Honda, Y.; Kitao, O.; Nakai, H.; Klene, M.; Li, X.; Knox, J. E.; Hratchian, H. P.; Cross, J. B.; Bakken, V.; Adamo, C.; Jaramillo, J.; Gomperts, R.; Stratmann, R. E.; Yazyev, O.; Austin, A. J.; Cammi, R.; Pomelli, C.; Ochterski, J. W.; Ayala, P. Y.; Morokuma, K.; Voth, G. A.; Salvador, P.; Dannenberg, J. J.; Zakrzewski, V. G.; Dapprich, S.; Daniels, A. D.; Strain, M. C.; Farkas, O.; Malick, D. K.; Rabuck, A. D.; Raghavachari, K.; Foresman, J. B.; Ortiz, J. V.; Cui, Q.; Baboul, A. G.; Clifford, S.; Cioslowski, J.; Stefanov, B. B.; Liu, G.; Liashenko, A.; Piskorz, P.; Komaromi, I.; Martin, R. L.; Fox, D. J.; Keith, T.; Al-Laham, M. A.; Peng, C. Y.; Nanayakkara, A.; Challacombe, M.; Gill, P. M. W.; Johnson, B.; Chen, W.; Wong, M. W.; Gonzalez, C.; Pople, J. A. *Gaussian 03*, revision E.01; Gaussian Inc.: Wallingford, CT, 2004.

(40) Mori, T.; Kobayashi, A.; Sasaki, Y.; Kobayashi, H.; Saito, G.; Inokuchi, H. *Bull. Chem. Soc. Jpn.* **1984**, *57*, 627−633.

(41) Aonuma, S.; Sawa, H.; Kato, R. *J. Chem. Soc., Perkin Trans. 2* **1995**, 1541−1549.

(42) Isono, T.; Kamo, H.; Ueda, A.; Takahashi, K.; Kimata, M.; Tajima, H.; Tsuchiya, S.; Terashima, T.; Uji, S.; Mori, H. *Phys. Rev. Lett.* **2014**, *112*, 177201.

(43) Bleaney, B.; Bowers, K. D. *Proc. R. Soc. London, Ser. A* **1952**, *214*, 451−465.

(44) Semmingsen, D.; Feder, J. *Solid State Commun.* **1974**, *15*, 1369−1372.

(45) Horiuchi, S.; Kumai, R.; Tokura, Y. *J. Am. Chem. Soc.* **2005**, *127*, 5010−5011.

(46) Seo, H.; Hotta, C.; Fukuyama, H. *Chem. Rev.* **2004**, *104*, 5005−5036.

(47) Miyagawa, K.; Kawamoto, A.; Kanoda, K. *Phys. Rev. B* **2000**, *62*, 7679−7682.

(48) Kimura, S.; Suzuki, H.; Maejima, T.; Mori, H.; Yamaura, J.; Kakiuchi, T.; Sawa, H.; Moriyama, H. *J. Am. Chem. Soc.* **2006**, *128*, 1456−1457.

(49) Matsushita, E.; Matsubara, T. *Prog. Theor. Phys.* **1982**, *67*, 1−19.

(50) Scheiner, S.; Čuma, M. *J. Am. Chem. Soc.* **1996**, *118*, 1511−1521.

(51) Some non-H-bonded organic materials also display thermal bistability in magnetic (and conductivity) channel(s). For example, see: (a) Barclay, T. M.; Cordes, A. W.; George, N. A.; Haddon, R. C.; Itkis, M. E.; Mashuta, M. S.; Oakley, R. T.; Patenaude, G. W.; Reed, R. W.; Richardson, J. F.; Zhang, H. *J. Am. Chem. Soc.* **1998**, *120*, 352−

360. (b) Fujita, W.; Awaga, K. *Science* **1999**, *286*, 261−262. (c) McManus, G. D.; Rawson, J. M.; Feeder, N.; van Duijn, J.; McInnes, E. J. L.; Novoa, J. J.; Burriel, R.; Palacio, F.; Oliete, P. *J. Mater. Chem.* **2001**, *11*, 1992−2003. (d) Itkis, M. E.; Chi, X.; Cordes, A. W.; Haddon, R. C. *Science* **2002**, *296*, 1443−1445. (e) Brusso, J. L.; Clements, O. P.; Haddon, R. C.; Itkis, M. E.; Leitch, A. A.; Oakley, R. T.; Reed, R. W.; Richardson, J. F. *J. Am. Chem. Soc.* **2004**, *126*, 8256−8265. A mechanism of this kind of hysteretic phase transition was discussed in terms of the intermolecular C-H···π distance change; see also: (f) Pal, S. K.; Bag, P.; Sarkar, A.; Chi, X.; Itkis, M. E.; Tham, F. S.; Donnadieu, B.; Haddon, R. C. *J. Am. Chem. Soc.* **2010**, *132*, 17258−17264.